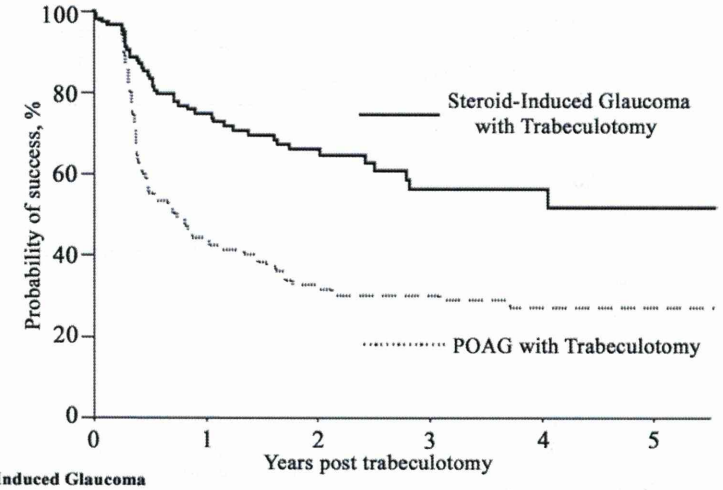

Steroid-Induced Glaucoma											
No. at risk	121	121	89	76	64	48	33	22	16	13	10
Failure	0	19	9	5	3	2	3	0	0	1	0
Censored	0	13	4	7	13	13	8	6	3	2	2
POAG											
No. at risk	108	108	57	45	37	28	24	22	17	16	12
Failure	0	47	11	6	5	2	0	1	1	0	0
Censored	0	4	1	2	4	2	2	4	0	4	3

FIGURE 2. Criterion B–based Kaplan-Meier survival curves of surgical outcomes in patients with steroid-induced glaucoma (solid line) vs primary open-angle glaucoma (POAG; dotted line) that underwent trabeculotomy. The steroid-induced glaucoma eyes had a significantly higher cumulative probability of success than the POAG eyes ($P < .0001$).

TABLE 2. Cox Proportional Hazards Model Determining Likelihood of Surgical Outcomes for Patients With Steroid-Induced Glaucoma and Primary Open-Angle Glaucoma who Underwent Trabeculotomy

	Criterion A			Criterion B		
Variable	RR	95% CI	*P* Value	RR	95% CI	*P* Value
Steroid-induced glaucoma	0.409	0.223–0.735	.0027	0.451	0.286–0.706	.0005
Age (per year)	0.999	0.982–1.015	.8917	1.007	0.995–1.019	.2408
Preoperative IOP (per mm Hg)	1.004	0.977–1.029	.7557	0.993	0.972–1.013	.5115
Female	0.761	0.451–1.260	.2911	0.695	0.468–1.021	.0639
Previous cataract surgery	2.105	0.823–4.681	.1132	1.627	0.784–3.084	.1804
Combined sinusotomy	1.054	0.575–1.847	.8600	0.839	0.526–1.300	.4399

CI = confidence interval; IOP = intraocular pressure; RR = relative risk.

Institute, Cary, North Carolina, USA). Comparisons of the outcomes between the steroid-induced glaucoma with trabeculotomy group and the POAG with trabeculotomy group, as well as between the steroid-induced glaucoma with trabeculotomy group and the steroid-induced glaucoma with trabeculectomy group, were analyzed by the Kaplan-Meier survival curve and the log-rank test. To assess prognostic factors of steroid-induced glaucoma with trabeculotomy in univariate analysis, Kaplan-Meier survival-curve analysis and the log-rank test were used. To confirm the effects of prognostic factors and to identify the relative risk (RR) of surgical failure, multivariate prognostic factor analysis was performed with the Cox proportional hazards model. Multivariate factors were selected from variants with a probability (P) value of less than .15 shown by univariate analysis. A P value less than .05 was considered statistically significant.

RESULTS

• PATIENT CHARACTERISTICS: In total, 163 patients (163 eyes) with steroid-induced glaucoma and 108 patients (108 eyes) with POAG satisfied the study criteria. All eligible patients were Japanese. Of the 163 eyes with steroid-induced glaucoma, 121 were included in the steroid-induced glaucoma with trabeculotomy group and 42 were included in the steroid-induced glaucoma with trabeculectomy group. Table 1 lists the characteristics of the enrolled patients.

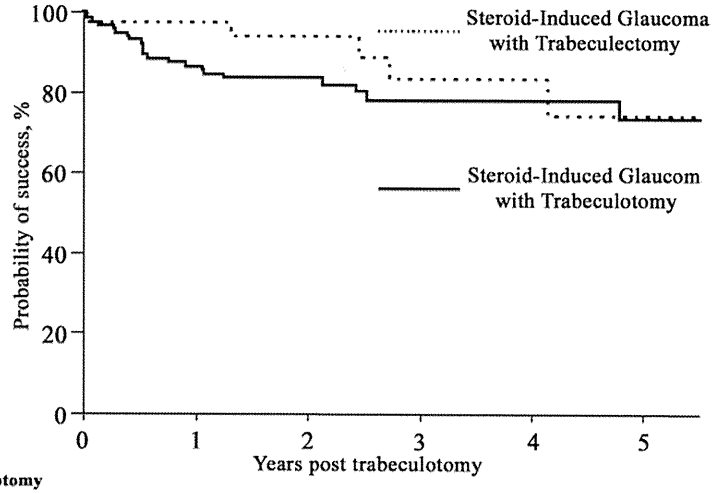

Trabeculotomy											
No. at risk	121	121	100	89	77	63	42	32	26	22	20
Failure	0	8	7	3	0	2	1	0	0	0	1
Censored	0	13	4	9	14	19	9	6	4	2	5
Trabeculectomy											
No. at risk	42	42	32	31	28	23	17	14	11	10	8
Failure	0	1	0	1	0	1	1	0	0	1	0
Censored	0	9	1	2	5	5	3	3	1	1	2

FIGURE 3. Criterion A–based Kaplan-Meier survival curves of surgical outcomes in eyes with trabeculotomy (solid line) vs trabeculectomy (dotted line) for steroid-induced glaucoma. There was no significant difference in the cumulative probability of success between the eyes with trabeculotomy and trabeculectomy (P = .3636).

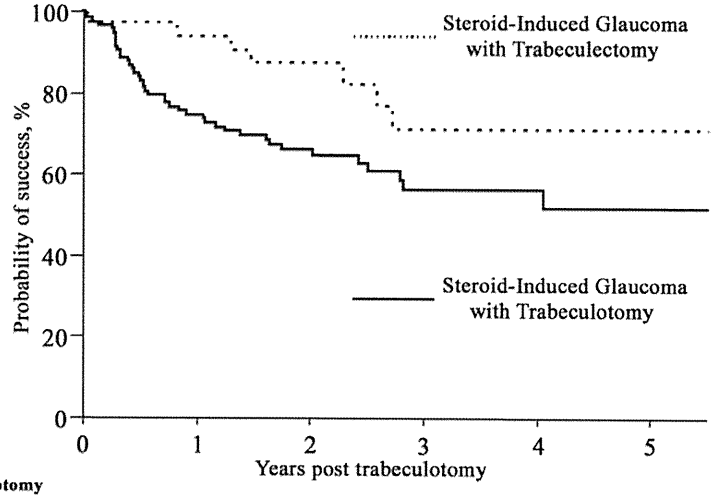

Trabeculotomy											
No. at risk	121	121	89	76	64	48	33	22	16	13	10
Failure	0	19	9	5	3	2	3	0	0	1	0
Censored	0	13	4	7	13	13	8	6	3	2	2
Trabeculectomy											
No. at risk	42	42	32	30	26	21	15	11	9	8	7
Failure	0	1	1	2	0	1	2	0	0	0	0
Censored	0	9	1	2	5	5	2	2	1	1	1

FIGURE 4. Criterion B–based Kaplan-Meier survival curves of surgical outcomes in eyes with trabeculotomy (solid line) vs trabeculectomy (dotted line) for steroid-induced glaucoma. The trabeculectomy group showed a significantly higher cumulative probability of success than the trabeculotomy group (P = .0352).

The steroid-induced glaucoma with trabeculotomy group was significantly younger ($P = .001$) and had a higher preoperative IOP ($P < .001$), a higher number of female patients ($P = .014$), a higher number of previous cataract surgeries ($P = .029$), and a lower number of combined sinusotomies ($P = .012$) than the POAG with

TABLE 3. Influence of Prognostic Factors on Survival Time of Steroid-Induced Glaucoma Patients who Underwent Trabeculotomy

Variable	Number of Patients	Criterion A		Criterion B	
		80% Survival Time (Days)	*P* Value[a]	80% Survival Time (Days)	*P* Value[a]
Gender			.1779		.0422
Female	62	>3850		305	
Male	59	385		146	
Age (years)			.9040		.2458
<30	51	852		206	
≥30	70	916		181	
Preoperative IOP (mm Hg)			.7443		.4387
<40	79	181		181	
≥40	42	840		200	
Diabetes mellitus			.1936		.0848
Yes	13	146		96	
No	108	816		291	
Hypertension			.9394		.9915
Yes	18	>2148		291	
No	103	852		195	
Combined sinusotomy			.2416		.9270
Yes	20	146		120	
No	101	916		260	
Previous cataract surgery			.0055		.1829
Yes	17	49		49	
No	104	1732		272	
Previous vitrectomy			<0.0001		.0050
Yes	6	10		10	
No	115	1742		260	
Cause of corticosteroid use					
Collagen disease			.3397		.9248
Yes	37	750		195	
No	84	1732		200	
Atopic dermatitis			.9929		.2449
Yes	21	278		162	
No	100	852		195	
Uveitis			.4674		.7942
Yes	25	>2519		177	
No	96	840		200	
Route of steroid administration					
Ocular instillation only			.6968		.1204
Yes	17	1732		1286	
No	104	852		181	
Posterior sub-Tenon's injection of TA			.9546		.3239
Yes	13	>1339		>1339	
No	108	916		200	
Intravitreal injection of TA			.1843		.4379
Yes	10	49		49	
No	111	916		206	
Oral administration			.7412		.6920
Yes	72	840		181	
No	49	1732		272	
Intravenous administration			.4050		.1883
Yes	3	>1580		>1580	
No	118	852		195	

Continued on next page

TABLE 3. Influence of Prognostic Factors on Survival Time of Steroid-Induced Glaucoma Patients who Underwent Trabeculotomy *(Continued)*

Variable	Number of Patients	Criterion A		Criterion B	
		80% Survival Time (Days)	*P* Value[a]	80% Survival Time (Days)	*P* Value[a]
Postoperative corticosteroid administration			.1987		.7335
>3 months	68	<3850		195	
≤3 months	53	372		200	

IOP = intraocular pressure; TA = triamcinolone acetonide.
[a]The *P* values are based on the log-rank test.

trabeculotomy group. However, there were no significant differences in patient characteristics between the steroid-induced glaucoma with trabeculotomy group and the steroid-induced glaucoma with trabeculectomy group.

• STEROID-INDUCED GLAUCOMA VS POAG: The mean follow-up periods were 38.4 ± 28.7 months in the steroid-induced glaucoma with trabeculotomy group and 49.8 ± 37.2 months in the POAG with trabeculotomy group (P = 0.010). Kaplan-Meier survival-curve analyses of the steroid-induced glaucoma with trabeculotomy group and the POAG with trabeculotomy group for criteria A and B are presented in Figures 1 and 2, respectively. The steroid-induced glaucoma with trabeculotomy group had a significantly higher cumulative probability of success for criteria A (P = .0008) and B (P < .0001). For criterion A, the probabilities of success 1, 2, 3, and 5 years after trabeculotomy in the steroid-induced glaucoma with trabeculotomy group and the POAG with trabeculotomy group were as follows: 86.5% vs 73.2%, 83.5% vs 63.0%, 78.1% vs 55.8%, and 73.5% vs 52.2%, respectively. For criterion B, the probabilities of success 1, 2, 3, and 5 years after trabeculotomy in the steroid-induced glaucoma with trabeculotomy group and the POAG with trabeculotomy group were as follows: 74.6% vs 44.7%, 66.1% vs 33.0%, 56.4% vs 30.6%, and 51.7% vs 27.5%, respectively. The number of eyes classified as surgical failures in the steroid-induced glaucoma with trabeculotomy group and the POAG with trabeculotomy group were 22/121 (18.2%) vs 45/108 (41.7%) for criterion A and 42/121 (34.7%) vs 73/108 (67.6%) for criterion B, respectively.

Since there were significant differences between the preoperative data of the steroid-induced glaucoma with trabeculotomy group and the POAG with trabeculotomy group, a Cox proportional hazards model including age, preoperative IOP, gender, previous cataract surgery, and combined sinusotomy was performed (Table 2). The multivariate model suggested that trabeculotomy in steroid-induced glaucoma eyes was independently associated with a better prognosis when compared with the same procedure in POAG eyes, even after adjusting for confounding factors (criterion A, RR = 0.409, P = .0027; criterion B, RR = 0.451, P = .0005).

• TRABECULOTOMY VS TRABECULECTOMY: The mean follow-up period in the steroid-induced glaucoma with trabeculectomy group was 37.1 ± 31.8 months (38.4 ± 28.7 months in the steroid-induced glaucoma with trabeculotomy group, P = .808). The Kaplan-Meier survival-curve analysis between the steroid-induced glaucoma with trabeculotomy group and the steroid-induced glaucoma with trabeculectomy group for criteria A and B are presented in Figures 3 and 4, respectively. No significant difference was found between the 2 groups for criterion A (P = .3636). The probabilities of success 1, 2, 3, and 5 years after surgery in the steroid-induced glaucoma with trabeculectomy group for criterion A were 97.6%, 94.3%, 83.8%, and 74.5%, respectively. The number of eyes classified as surgical failures in the steroid-induced glaucoma with trabeculectomy group was 5 (11.9%) for criterion A. However, the steroid-induced glaucoma with trabeculectomy group showed a significantly higher cumulative probability of success for criterion B (P = .0352). The probabilities of success 1, 2, 3, and 5 years after surgery in the steroid-induced glaucoma with trabeculectomy group for criterion B were 94.5%, 87.7%, 71.6%, and 71.6%, respectively. The number of eyes classified as surgical failures in the steroid-induced glaucoma with trabeculectomy group was 7 (16.7%) for criterion B.

• PROGNOSTIC FACTORS FOR FAILURE OF TRABECULOTOMY FOR STEROID-INDUCED GLAUCOMA EYES: The potential prognostic factors influencing survival time are listed in Table 3. Univariate analysis showed previous cataract surgery (P = .0055) and previous vitrectomy (P < .0001) to be significant prognostic factors for criterion A, and male gender (P = .0422) and previous vitrectomy (P = .0050) for criterion B. Diabetes mellitus (P = .0848) and ocular instillation of corticosteroid (P = .1204) were the factors with a P value of less than .15 for criterion B. The Cox proportional hazards model including these variables revealed that prognostic factors for surgical failure were

TABLE 4. Cox Proportional Hazards Model on Criteria A and B, Determining Likelihood of Surgical Outcomes for All 121 Patients With Steroid-Induced Glaucoma who Underwent Trabeculotomy

Variable	Criterion A			Criterion B		
	RR	95% CI	*P* Value	RR	95% CI	*P* Value
Previous cataract surgery	1.614	0.255–5.688	.5488		—	
Previous vitrectomy	5.340	1.037–38.655	.0452	3.898	1.108–10.688	.0360
Male		—		1.783	0.938–3.414	.0774
Diabetes mellitus		—		1.871	0.754–4.018	.1632
Corticosteroid administration other than ocular instillation		—		2.752	1.065–9.426	.0352

CI = confidence interval; IOP = intraocular pressure; RR = relative risk.

previous vitrectomy (RR = 5.340, P = .0452 for criterion A; RR = 3.898, P = .0360 for criterion B) and corticosteroid administration other than ocular instillation (RR = 2.752, P = .0352 for criterion B) (Table 4).

• POSTOPERATIVE COMPLICATIONS: In the steroid-induced glaucoma with trabeculectomy group, choroidal detachment occurred in 2 eyes (4.8%), flat anterior chamber requiring anterior chamber reformation occurred in 1 eye (2.4%), and hypotony maculopathy occurred in 7 eyes (16.7%). None of these complications occurred in either the steroid-induced glaucoma with trabeculotomy group or the POAG with trabeculotomy group. The progression of postoperative cataracts was observed in 9 eyes (7.4%) of the steroid-induced glaucoma with trabeculotomy group, 1 eye (0.9%) of the POAG with trabeculotomy group, and 4 eyes (9.5%) of the steroid-induced glaucoma with trabeculectomy group. No eyes encountered postoperative infectious blebitis or endophthalmitis.

DISCUSSION

THIS STUDY COMPARED THE SUCCESS RATES OF TRABECULotomy for steroid-induced glaucomatous eyes with those for trabeculectomy for steroid-induced glaucoma eyes, and for trabeculotomy for POAG eyes. Trabeculotomy showed a significantly higher cumulative probability of success in steroid-induced glaucoma patients than POAG patients for both criterion A (P = .0008) and criterion B (P < .0001). The probability of success in steroid-induced glaucoma eyes treated with trabeculotomy was comparable to that in steroid-induced glaucoma eyes treated with MMC trabeculectomy for criterion A (P = .3636), but was significantly lower for criterion B (P = .0352). Significant prognostic factors for surgical failure of trabeculotomy in steroid-induced glaucoma patients were previous vitrectomy for criteria A (RR = 5.340, P = .0452) and B (RR = 3.898, P = .0360), and corticosteroid treatment other than ocular instillation for criterion B (RR = 2.752, P = .0352).

Several studies have demonstrated surgical results for steroid-induced glaucoma patients.[10,11,13–15,17,23–27] For example, Sihota and associates[10] reported that 9 eyes with steroid-induced glaucoma that required trabeculectomy with MMC showed normal IOP levels after surgery. Several reports[11,23–27] demonstrated that filtering surgery was successful for IOP management in steroid-induced glaucomatous eyes after intravitreal injection of triamcinolone acetonide. Krishnan and associates[13] found that all of 3 eyes with triamcinolone-induced IOP elevation were successfully treated with viscocanalostomy. For laser trabeculoplasty, Ricci and associates[14] and Viola and associates[15] reported that argon laser trabeculoplasty was effective in all cases in their studies, and selective laser trabeculoplasty was shown to lower IOP in 5 of 7 eyes.[17] However, these reports on surgical treatment for steroid-induced glaucoma included only a small number of cases and lacked control groups and details of long-term prognosis. Our previous study lacked control groups but showed that trabeculotomy reduced IOPs to 21 mm Hg or less in 14 eyes with steroid-induced glaucoma.[12] To our knowledge, our present multicenter study reports on the largest number of steroid-induced glaucoma patients.

Trabeculotomy showed a better prognosis in steroid-induced glaucoma eyes than POAG eyes in the present study. The accumulation of extracellular matrices in trabecular meshwork has been believed to cause increased outflow resistance of the aqueous humor in steroid-induced glaucoma patients. This is because histochemical data demonstrate abnormally accumulated extracellular matrices such as type IV collagen, heparin sulfate, proteoglycan, and fibronectin in the trabecular meshwork of steroid-induced glaucoma patients.[9] Because the main target of trabeculotomy for IOP reduction is the relief of outflow resistance in the trabecular meshwork, the consistency between the surgical target and the pathologic lesion might explain the effectiveness of surgery for steroid-induced glaucoma eyes.

The surgical success of trabeculotomy for steroid-induced glaucoma was comparable to the success of MMC trabeculectomy for steroid-induced glaucoma for criterion

A. Trabeculectomy has a potential risk of late-onset infection of the filtering bleb.[28–31] A previous multicenter case-control study suggested that the use of systemic corticosteroid and juvenile-onset glaucoma should be included among the risk factors for late-onset infection after filtering surgery.[32] Moreover, younger patients are more susceptible to steroid-induced IOP elevation.[4,33,34] Trabeculotomy might be more beneficial for younger patients with steroid-induced glaucoma, from the viewpoint of late-onset infection, than trabeculectomy because of the nonfiltering surgery.

Trabeculectomy had a significantly higher probability of success than trabeculotomy using criterion B in the present study. Thus, many steroid-induced glaucoma eyes treated with trabeculotomy had postoperative IOPs of 18 to 20 mm Hg, which might be too high to prevent progressive visual field changes for glaucomatous eyes with advanced progressive visual field defects. The Advanced Glaucoma Intervention Study[35] found that visual field loss in eyes with advanced open-angle glaucoma progresses further if postoperative IOP of 18 mm Hg or higher is more frequent. These findings imply that trabeculectomy rather than trabeculotomy is more favorable for controlling IOP in steroid-induced glaucoma eyes with advanced visual field loss.

Even when other types of glaucoma are included, the prognostic factors for the surgical failure of trabeculotomy have not been sufficiently identified. Our previous report indicated that higher preoperative IOP results in poorer prognosis in eyes with POAG or exfoliative glaucoma.[19] Higher preoperative IOP might reflect the severity of glaucoma, resulting in a poorer response to reduce IOP. The present study showed that higher preoperative IOP was not a prognostic factor for surgical failure of trabeculotomy for steroid-induced glaucoma, while corticosteroid administration other than ocular instillation was shown to be a prognostic factor in criterion B. These data might reflect the fact that the severity of steroid-induced glaucoma depends on the route of corticosteroid administration rather than the preoperative IOP levels. In addition, previous vitrectomy was a prognostic factor for surgical failure for both criteria. Although we have no conclusive explanation, it is conceivable that vitrectomy causes the elevation of inflammatory factors or growth factors in the aqueous humor. Vitrectomized eyes might lead to recurrent fibrosis in the outflow pathway of the trabecular meshwork that was created by the trabeculotomy.

This study had some limitations caused by the retrospective design. First, the selection bias of the type of surgery performed for steroid-induced glaucoma eyes might have affected the surgical result. In fact, all 6 vitrectomized eyes were treated with trabeculotomy. Because of conjunctival scarring after vitrectomy, trabeculotomy rather than trabeculectomy might have been the surgery of choice for vitrectomized eyes. Second, as higher IOP is a prognostic factor for failure of trabeculotomy for POAG eyes,[19] POAG patients with higher IOP might have been treated with trabeculectomy rather than trabeculotomy; this might have increased the cumulative probability of success in POAG with trabeculotomy.

In conclusion, this study demonstrates that trabeculotomy might be more effective for steroid-induced glaucoma eyes than POAG eyes. Moreover, the surgical success in steroid-induced glaucoma eyes is comparable to the outcome of trabeculectomy unless more substantial IOP reduction is necessary, in which case trabeculectomy would be a better option. IOP reduction of steroid-induced glaucoma patients with previous vitrectomy or with corticosteroid administration other than ocular instillation might be more resistant to trabeculotomy. Trabeculotomy should be considered as an option for the surgical management of steroid-induced glaucoma, although future prospective studies are necessary to validate our findings.

PUBLICATION OF THIS ARTICLE WAS SUPPORTED, IN PART, BY GRANTS-IN-AID FOR SCIENTIFIC RESEARCH FROM THE Ministry of Education, Culture, Sports, Science and Technology (MEXT), Tokyo, Japan, and the Suda Memorial Glaucoma Treatment Research Foundation, Tokyo, Japan. The authors indicate no financial conflict of interest. Involved in design and conduct of the study (K.I., M.I., H.T.); collection and management of the data (all authors); analysis (K.I., M.I); interpretation of the data (all authors); preparation of the first draft of the manuscript (K.I., M.I); and review and approval of the manuscript (all authors). All procedures conformed to the Declaration of Helsinki and informed consent was obtained from each of the patients participating in the study. The multicenter retrospective study protocol was approved by the Institutional Review Board of Kumamoto University Hospital, Kumamoto City, Japan.

Members of the Japanese Steroid-Induced Glaucoma Multicenter Study Group: *Kumamoto University Graduate School of Medical Sciences, Kumamoto, Japan:* Keiichiro Iwao, Masaru Inatani, and Hidenobu Tanihara. *Saga University Faculty of Medicine, Saga, Japan:* Keiichiro Iwao, Shinichiro Ishikawa, and Satoshi Okinami. *Graduate School of Medical and Dental Sciences, Niigata University, Niigata, Japan:* Takayuki Tanaka and Takeo Fukuchi. *University of Tokyo, Graduate School of Medicine, Tokyo, Japan:* Makiko Ito and Toshikatsu Kaburaki. *Kanazawa University Graduate School of Medical Science, Kanazawa, Japan:* Eiji Murotani and Tomomi Higashide. *Gifu University Graduate School of Medicine, Gifu, Japan:* Kyoko Ishida and Tetsuya Yamamoto. *Kagawa University Faculty of Medicine, Kagawa, Japan:* Kazuyuki Hirooka and Fumio Shiraga. *Faculty of Medicine, University of Yamanashi, Yamanashi, Japan:* Kiyotaka Ishijima and Kenji Kashiwagi. *Tohoku Graduate School of Medicine, Sendai, Japan:* Toru Nakazawa and Nobuo Fuse. *Ryukyu University School of Medicine, Okinawa, Japan:* Eriko Tomoyose and Hiroshi Sakai. *Kyoto Prefectural University of Medicine, Kyoto, Japan:* Yoko Ikeda and Kazuhiko Mori. *Kagoshima University Graduate School of Medical and Dental Sciences, Kagoshima, Japan:* Takehiro Yamashita and Taiji Sakamoto. *Kyoto University Graduate School of Medicine, Kyoto, Japan:* Fumitaka Hirose and Masanori Hangai. *Nagoya City University Graduate School of Medical Sciences, Nagoya, Japan:* Miho Nozaki and Yuichiro Ogura. *Kobe University Graduate School of Medicine, Hyogo, Japan:* Maiko Naka and Akira Negi. *Graduate School of Biomedical Sciences, Hiroshima University, Japan:* Mina Mizukami and Takashi Kanamoto. *NTT West Kyusyu Hospital, Kumamoto, Japan:* Ryusuke Futa.

REFERENCES

1. Lewis JM, Priddy T, Judd J, et al. Intraocular pressure response to topical dexamethasone as a predictor for the development of primary open-angle glaucoma. Am J Ophthalmol 1988;106(5):607–612.
2. Jonas JB, Kreissig I, Degenring R. Secondary chronic open-angle glaucoma after intravitreal triamcinolone acetonide. Arch Ophthalmol 2003;121(5):729–730.
3. Smithen LM, Ober MD, Maranan L, Spaide RF. Intravitreal triamcinolone acetonide and intraocular pressure. Am J Ophthalmol 2004;138(5):740–743.
4. Iwao K, Inatani M, Kawaji T, Koga T, Mawatari Y, Tanihara H. Frequency and risk factors for intraocular pressure elevation after posterior sub-Tenon capsule triamcinolone acetonide injection. J Glaucoma 2007;16(2):251–256.
5. Opatowsky I, Feldman RM, Gross R, Feldman ST. Intraocular pressure elevation associated with inhalation and nasal corticosteroids. Ophthalmology 1995;102(2):177–179.
6. Becker B, Mills D. Corticosteroids and intraocular pressure. Arch Ophthalmol 1963;70(4):500–507.
7. Rohen JW, Linner E, Witmer R. Electron microscopic studies on the trabecular meshwork in two cases of corticosteroid-glaucoma. Exp Eye Res 1973;17(1):19–31.
8. Johnson D, Gottanka J, Flugel C, Hoffmann F, Futa R, Lutjen-Drecoll E. Ultrastructural changes in the trabecular meshwork of human eyes treated with corticosteroids. Arch Ophthalmol 1997;115(3):375–383.
9. Tawara A, Tou N, Kubota T, Harada Y, Yokota K. Immunohistochemical evaluation of the extracellular matrix in trabecular meshwork in steroid-induced glaucoma. Graefes Arch Clin Exp Ophthalmol 2008;246(7):1021–1028.
10. Sihota R, Konkal VL, Dada T, Agarwal HC, Singh R. Prospective, long-term evaluation of steroid-induced glaucoma. Eye (Lond) 2008;22(1):26–30.
11. Jonas JB, Degenring RF, Kamppeter BA. Outcome of eyes undergoing trabeculectomy after intravitreal injections of triamcinolone acetonide. J Glaucoma 2004;13(3):261.
12. Honjo M, Tanihara H, Inatani M, Honda Y. External trabeculotomy for the treatment of steroid-induced glaucoma. J Glaucoma 2000;9(6):483–485.
13. Krishnan R, Kumar N, Wishart PK. Viscocanalostomy for refractory glaucoma secondary to intravitreal triamcinolone acetonide injection. Arch Ophthalmol 2007;125(9):1284–1286.
14. Ricci F, Missiroli F, Parravano M. Argon laser trabeculoplasty in triamcinolone acetonide induced ocular hypertension refractory to maximal medical treatment. Eur J Ophthalmol 2006;16(5):756–757.
15. Viola F, Morescalchi F, Staurenghi G. Argon laser trabeculoplasty for intractable glaucoma following intravitreal triamcinolone. Arch Ophthalmol 2006;124(1):133–134.
16. Pizzimenti JJ, Nickerson MM, Pizzimenti CE, Kasten-Aker AG. Selective laser trabeculoplasty for intraocular pressure elevation after intravitreal triamcinolone acetonide injection. Optom Vis Sci 2006;83(7):421–425.
17. Rubin B, Taglienti A, Rothman RF, Marcus CH, Serle JB. The effect of selective laser trabeculoplasty on intraocular pressure in patients with intravitreal steroid-induced elevated intraocular pressure. J Glaucoma 2008;17(4):287–292.
18. Baser E, Seymenoglu R. Selective laser trabeculoplasty for the treatment of intraocular pressure elevation after intravitreal triamcinolone injection. Can J Ophthalmol 2009;44(3):e21.
19. Tanihara H, Negi A, Akimoto M, et al. Surgical effects of trabeculotomy ab externo on adult eyes with primary open angle glaucoma and pseudoexfoliation syndrome. Arch Ophthalmol 1993;111(12):1653–1661.
20. Sugimoto-Takeuchi R, Kuwayama Y, Shiga S, Takagi T. Trabeculotomy for steroid glaucoma. Atarashii Ganka (Journal of the Eye) 1992;9(7):1181–1183.
21. Mizoguchi T, Nagata M, Matsumura M, Kuroda S, Terauchi H, Tanihara H. Surgical effects of combined trabeculotomy and sinusotomy compared to trabeculotomy alone. Acta Ophthalmol Scand 2000;78(2):191–195.
22. Cairns JE. Trabeculectomy. Preliminary report of a new method. Am J Ophthalmol 1968;66(4):673–679.
23. Park HY, Yi K, Kim HK. Intraocular pressure elevation after intravitreal triamcinolone acetonide injection. Korean J Ophthalmol 2005;19(2):122–127.
24. Quiram PA, Gonzales CR, Schwartz SD. Severe steroid-induced glaucoma following intravitreal injection of triamcinolone acetonide. Am J Ophthalmol 2006;141(3):580–582.
25. Kubota T, Okabe H, Hisatomi T, Yamakiri K, Sakamoto T, Tawara A. Ultrastructure of the trabecular meshwork in secondary glaucoma eyes after intravitreal triamcinolone acetonide. J Glaucoma 2006;15(2):117–119.
26. Kaushik S, Gupta V, Gupta A, Dogra MR, Singh R. Intractable glaucoma following intravitreal triamcinolone in central retinal vein occlusion. Am J Ophthalmol 2004;137(4):758–760.
27. Singh IP, Ahmad SI, Yeh D, et al. Early rapid rise in intraocular pressure after intravitreal triamcinolone acetonide injection. Am J Ophthalmol 2004;138(2):286–287.
28. Lobue TD, Deutsch TA, Stein RM. Moraxella nonliquefaciens endophthalmitis after trabeculectomy. Am J Ophthalmol 1985;99(3):343–345.
29. Freedman J, Gupta M, Bunke A. Endophthalmitis after trabeculectomy. Arch Ophthalmol 1978;96(6):1017–1018.
30. Higginbotham EJ, Stevens RK, Musch DC, et al. Bleb-related endophthalmitis after trabeculectomy with mitomycin C. Ophthalmology 1996;103(4):650–656.
31. Wolner B, Liebmann JM, Sassani JW, Ritch R, Speaker M, Marmor M. Late bleb-related endophthalmitis after trabeculectomy with adjunctive 5-fluorouracil. Ophthalmology 1991;98(7):1053–1060.
32. Jampel HD, Quigley HA, Kerrigan-Baumrind LA, Melia BM, Friedman D, Barron Y. Risk factors for late-onset infection following glaucoma filtration surgery. Arch Ophthalmol 2001;119(7):1001–1008.
33. Inatani M, Iwao K, Kawaji T, et al. Intraocular pressure elevation after injection of triamcinolone acetonide: a multicenter retrospective case-control study. Am J Ophthalmol 2008;145(4):676–681.
34. Ohji M, Kinoshita S, Ohmi E, Kuwayama Y. Marked intraocular pressure response to instillation of corticosteroids in children. Am J Ophthalmol 1991;112(4):450–454.
35. The Advanced Glaucoma Intervention Study (AGIS): 7. The relationship between control of intraocular pressure and visual field deterioration. The AGIS Investigators. Am J Ophthalmol 2000;130(4):429-440.

Biosketch

Keiichiro Iwao, MD, PhD, received his doctorate from Saga University's Graduate School of Medicine, Saga, Japan, in 2009, which was based on mouse models of developmental glaucoma. He is currently assistant professor in the Department of Ophthalmology, Saga University Faculty of Medicine. He has been recognized by the Association for Research in Vision and Ophthalmology and was a recipient of the 2009 Kowa Travel Grant Award. His interests include glaucoma surgery and regeneration of the optic nerve.

JACS
JOURNAL OF THE AMERICAN CHEMICAL SOCIETY

ARTICLE

pubs.acs.org/JACS

Self-Regulating Enzyme–Nanotube Ensemble Films and Their Application as Flexible Electrodes for Biofuel Cells

Takeo Miyake,[†,§] Syuhei Yoshino,[†] Takeo Yamada,[‡,§] Kenji Hata,[‡,§] and Matsuhiko Nishizawa*[,†,§]

[†]Department of Bioengineering and Robotics, Tohoku University, 6-6-1 Aramaki Aoba, Aoba-ku, Sendai 980-8579, Japan

[‡]Nanotube Institute of Advanced Industrial Science and Technology (AIST), Tsukuba Central 5, 1-1-1 Higashi, Tsukuba, Ibaraki 308-8565, Japan

[§]Core Research for Evolutional Science and Technology (CREST), Japan Science and Technology Agency (JST), Tokyo 102-0075, Japan

Supporting Information

ABSTRACT: Nanostructured carbons have been widely used for fabricating enzyme-modified electrodes due to their large specific surface area. However, because they are random aggregates of particular or tubular nanocarbons, the postmodification of enzymes to their intrananospace is generally hard to control. Here, we describe a free-standing film of carbon nanotube forest (CNTF) that can form a hybrid ensemble with enzymes through liquid-induced shrinkage. This provides in situ regulation of its intrananospace (inter-CNT pitch) to the size of enzymes and eventually serves as a highly active electrode. The CNTF ensemble with fructose dehydrogenase (FDH) showed the oxidation current density of 16 mA cm^{-2} in stirred 200 mM fructose solution. The power density of a biofuel cell using the FDH–CNTF anode and the Laccase–CNTF cathode reached 1.8 mW cm^{-2} (at 0.45 V) in the stirred oxygenic fructose solution, more than 80% of which could be maintained after continuous operation for 24 h. Application of the free-standing, flexible character of the enzyme–CNTF ensemble electrodes is demonstrated via their use in the patch or wound form.

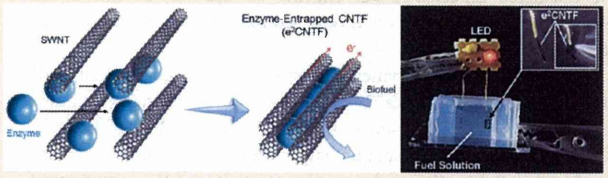

INTRODUCTION

Enzyme-modified electrodes are core components of bioelectronic devices, such as biofuel cells, which have attracted attention as safe power sources, generating electricity from natural fuels, like sugars and alcohols.[1−13] A variety of nanoengineered carbon electrodes for biofuel cells have recently been developed in rapid succession. The carbon nanotube (CNT)-based microfiber electrode is a cutting-edge example that improves a glucose biofuel cell to achieve a power of 0.74 mW cm^{-2} even in physiological, quiescent conditions.[11] Another noteworthy development is the careful control of the intrapore size of carbon cryogel that resulted in a high-power fructose fuel cell producing 0.85 mW cm^{-2} under stirred conditions.[12] The optimized nanopores can be expected to support the activity and the stability of enzymes.[14] However, all attempts to incorporate nanoengineered carbon electrodes have focused on prestructuring electrodes before enzyme modification. This is because the process for engineering carbon is bioincompatible due to the use of organic solvents or heating. If the nanostructure of the electrode can be regulated in response to the enzyme to be immobilized, then the resultant enzymatic ensemble would avoid the difficulty in postmodification of enzymes.

We present here a method to achieve ideal enzyme electrodes having suitable intrananospace automatically regulated to the size of enzymes. We utilize a carbon nanotube forest (CNTF) consisting of extremely long (~1 mm) single-walled CNTs,[15] which can be handled with tweezers, as a 100% binder-free carbon film. When liquids are introduced into the as-grown CNTF (CNTs with a pitch of 16 nm) and dried, the CNTF shrinks to a near-hexagonal close-packed structure (CNTs with a pitch of 3.7 nm) because of the surface tension of the liquids.[16,17] By using an enzyme solution as the liquid, the CNTF is expected to dynamically entrap the enzymes during the shrinkage, as illustrated in Figure 1. This "in-situ regulation" approach has led to reproducible activity of enzyme electrodes, to the first free-standing flexible character, and to high-power density biofuel cells.

EXPERIMENTAL SECTION

Preparation of Enzyme–Nanotube Ensemble Electrodes.

CNTF was synthesized in a 1-in. tube furnace by water-assisted chemical vapor deposition at 750 °C with a C_2H_4 carbon source and an Al_2O_3 (10 nm)/Fe (1 nm) thin-film catalyst grown on silicon wafers.[15,16] We used He with H_2 as the carrier gas [total flow 1000 standard cubic centimeters per minute (sccm)] at 1 atm with a controlled amount of water vapor with ethylene (100 sccm) for 10 min. The synthesized CNTF (1 mm × 1 mm) could be pulled from the substrate with tweezers (Supporting Information, Figure S1). The film thickness was set to 4 and 12 or 20 μm by the width of line-patterns of the catalyst. The CNTF film

Received: January 5, 2011
Published: March 10, 2011

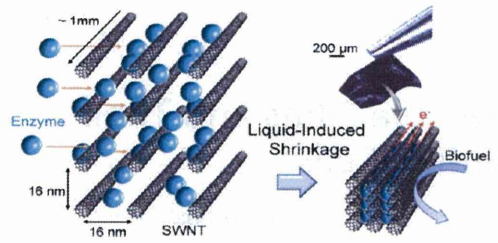

Figure 1. Schematic diagram of enzyme entrapment inside a CNTF by liquid-induced shrinkage. The photograph shows a free-standing enzyme−CNTF ensemble film that can be manipulated with tweezers.

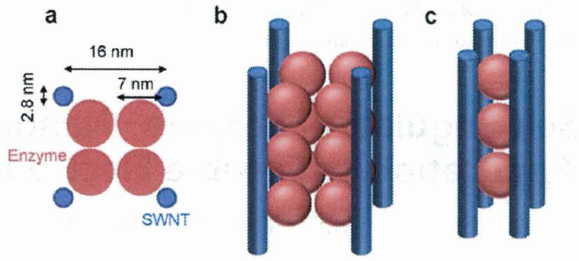

Figure 2. (a and b) Illustrations of as-grown CNTF whose void volume is fully occupied by 7 nm diameter globular enzyme molecules. (c) Illustration of the linear arrangement of the enzymes trapped between the shrunk CNTF.

was evaluated by the Brunauer−Emmett−Teller (BET) analysis of N_2 adsorption and the cyclic voltammetry in McIlvaine buffer (pH 5.0) at 10 mV s^{-1}; the resulting specific surface area and the specific capacitance of the film were approximately 1300 m^2 g^{-1} and 400 F g^{-1}, respectively. The calculated capacitance per effective surface area is thus ca. 30 μF cm^{-2} in agreement with that reported for highly oriented pyrolytic graphite (HOPG).[18]

We used two model enzymes: D-fructose dehydrogenase (FDH; EC 1.1.99.11, 169.9 U mg^{-1}, ca. 140 kDa, from *Gluconobacter*, purchased from Toyobo Enzyme Co.) and laccase (LAC; EC 1.10.3.2, 108 U mg^{-1}, ca. 60 kDa, from *Trametes* sp, purchased from Daiwa Kasei Co.), which can directly catalyze the oxidation of D-fructose and the reduction of dioxygen, respectively.[12] The FDH was used as received without further purification. The LAC was purified by anion exchange chromatography with a DEAE−Toyopearl column.[12] The size of the FDH can be assumed similar to that of 160 kDa glucose oxidase (7 × 5.5 × 8 nm).[19] In fact, the atomic force microscopy (AFM) showed ca. 7 nm bumpy structure for an FDH-adsorbed surface.[20] On the other hand, the LAC has dimensions of 6.5 × 5.5 × 4.5 nm.[21]

The CNTF film was first treated by 0.1% Triton X-100 and then immersed in a stirred McIlvaine buffer (pH 5.0) containing FDH for 1 h to introduce enzymes into its void space. After being washed three times, the CNTF film was placed on a carbon paper and dried in air, typically for 15 min. For cathode preparation, the CNTF film was immersed in 0.25 mg mL^{-1} (4.3 μM) LAC in McIlvaine buffer (pH 5.0) and stirred for 10 min, followed by drying on a carbon paper.

Quantitative Analysis of the Entrapped Enzymes. The enzyme-immobilized CNTF film was washed and immersed in 20 mM sodium phosphate buffer (pH 9.3) containing 0.1 M sodium borate and 1% sodium cholate and dispersed with an ultrasonic homogenizer for 15 min. The FDH in the dispersion was then analyzed using a C-6667 Protein Quantitation Kit (Molecular Probes), using 5 mM (3-(4-carboxybenzoyl)-quinoline-2-carboxaldehyde) (ATTO-TAG CBQCA) and 20 mM KCN to label the enzyme with CBQCA. After 1.5 h of incubation, the fluorescent intensity was measured by a luminescent image analyzer system (Fuji Photo Film, LAS-3000 mini), and the amount of enzyme was determined by referencing a calibration curve.

Theoretical Prospect of FDH Content inside CNTF. The previous structural analysis of the as-grown CNTF revealed a mean tube diameter of 2.8 nm by transmission electron microscopy (TEM) and an intertube pitch of 16 nm by X-ray diffraction (XRD).[16,17] If we assume that FDH is a 7 nm diameter globe, four FDHs can enter the void space surrounded by 16 nm pitched CNTs (Figure 2a and b). The number of enzymes (N_{enz}) entrapped in a 12 μm thick CNTF is estimated by the following equation: $N_{enz} = 4\ (H/r)\ (S/U)$, where H = 1.0 mm (CNT length), $r = 7.0 \times 10^{-6}$ mm (FDH diameter), $S = 12 \times 10^{-3}$ mm^2 (cross-sectional area of CNTF sheet), and $U = 2.6 \times 10^{-10}$ mm^2 (the area of the void space surrounded by 16 nm pitched CNTs). The entrapped mass (6.2 μg) is derived by multiplying N_{enz} by the molecular weight (140 kD)/Avogadro's constant. On the other hand, as we explain later in the Results and Discussion Section, the best performance of FDH−CNTF ensemble was obtained by the film containing ca. 1.5 μg FDH (one-quarter of the limiting value, 6.2 μg) (Figure 2c). Note these arguments are based on the assumption that FDH is a 7 nm diameter globe.

Electrochemical Measurements. The enzyme−CNTF ensemble film, anchored at the edge with SUS316L fine tweezers, was analyzed by a three-electrode system (BSA, 730C electrochemical analyzer) in stirred solutions using a Ag/AgCl reference and a platinum counter electrode. The catalytic currents of enzyme−CNTF ensemble films did not significantly decrease when the film was attached to a planner electrode (Supporting Information, Figure S2). We therefore used the area of one side of the film for the calculation of the current and power densities. The performance of a biofuel cell constructed from an FDH-based anode and an LAC-based cathode was evaluated on the basis of the cell voltage upon changing the external resistance between 1 kΩ and 2 MΩ (1.0, 5.1, 10.8, 15.8, 24.5, 35.3, 55.3, 100, 196, 500, 1000, and 2000 kΩ) at the time step of 60 s. Unless otherwise indicated, the electrochemical measurements were carried out at room temperature (25 °C). Although the apparent Michaelis−Menten constant ($K_{m,app}$) of the entrapped FDH is around 10 mM as we estimated later, we used 200 mM fructose solution in order to evaluate the cell performance in the high enough concentration of fuel and to compare the performance with previous works[12] under similar conditions.

LED Device Experiments. The LED device consisted of a charge pump IC (S-882Z20, input voltage [0.3−3 V), output voltage (V_{IC}, 2 V)], a 1 μF ceramic capacitor (C), and a red LED. The interval of the LED blink is the time required to charge the capacitor, which is described by

$$t = \frac{J}{P} = \frac{\frac{CV_{IC}^2}{2} - \frac{CV_{LED}^2}{2}}{I \times V_{cell}} \quad (1)$$

where J is the practical energy for the LED device operation, P is the cell power, V_{LED} is the operation voltage (1.6 V) of the LED, I is the cell current, and V_{cell} is the cell voltage; thus, the time interval (t) is inversely proportional to the power of the biofuel cell.

RESULTS AND DISCUSSION

Entrapment of Enzymes inside Self-Regulating Nanostructure of CNTF Films. The initial step of the entrapment process depends on sufficient loading of enzymes inside the as-grown 16 nm pitch CNTF film. As shown in Figure 3a, the in situ monitoring of electrocatalytic activity of the CNTF films on soaking in a buffer containing 3 mg mL^{-1} FDH with 200 mM D-fructose showed currents corresponding to their thickness (80

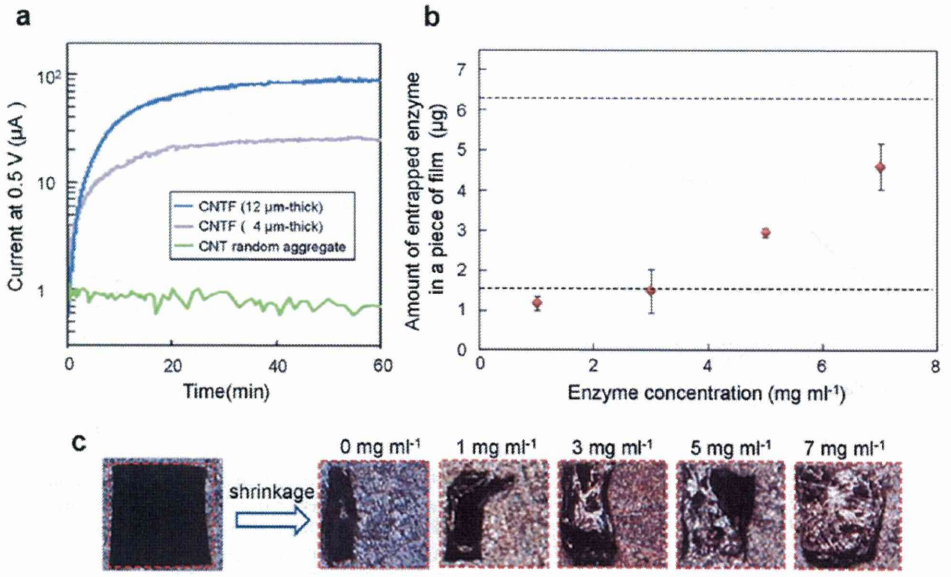

Figure 3. (a) The monitoring of the oxidation current at 0.5 V vs Ag/AgCl in a stirred McIlvaine buffer (pH 5.0) containing 3 mg mL^{-1} FDH and 200 mM fructose for the 4 and 12 μm thick CNTF films (1 × 1 mm), and a random CNT aggregate prepared by casting a CNTs' dispersion on an 1 × 1 mm Au electrode. (b) The relationship between the amount of entrapped FDH inside a piece of 12 μm thick CNTF film and the concentration of FDH solution in which the CNTFs were soaked for 1 h before the shrinkage. The experiments were carried out three times for each condition. (c) Photographs of CNTF films shrunk after soaking in different concentrations of FDH. For reference, the dashed square measures 1 × 1 mm.

μA for 12 μm thick film and 25 μA for 4 μm thick film), indicating that the FDH molecule can entirely penetrate inside the CNTF films. On the other hand, the catalytic activity of the conventional random CNT electrode, which was prepared by casting a CNTs' dispersion, remained around 1 μA despite having a large effective surface area comparable to that of the 4 μm thick CNTF film (both showed capacitance per geometric area of around 5 mF cm^{-2}). The results obtained from the random CNT electrode demonstrate the general difficulty in postmodification of enzymes to the prestructured nanocarbon electrodes, which will be addressed by the present "in-situ regulation" approach.

The content of FDH inside a CNTF film was controllable by the concentration of FDH solution in which the as-grown CNTF films were soaked for 1 h (Figure 3b). The FDH content increased toward the theoretical limiting value (6.2 μg), at which the void volume of as-grown CNTF is fully occupied by FDH (Figure 2). Such controlled entrapment of enzymes can be also examined via the degree of CNTF shrinkage (Figure 3c). Typically, the CNTF film without enzymes shrank to one-quarter of its original area; the CNTF film treated with 3 mg mL^{-1} FDH solution shrank to one-half of the original. The degree of shrinkage also depended on the size of enzyme. For example, a smaller enzyme, laccase, led to shrinkage to one-third of the original area. These results support our methodology, which induces in situ regulation of intrananospace of CNTF by the amount and size of entrapped enzymes. We refer to the enzyme-entrapped CNTF as "e^2CNTF". The enzyme-containing CNTF before shrinkage (before drying), in which enzymes simply adsorbed on CNTs' sidewall, is denoted as "eCNTF".

Electrocatalytic Activity of Enzyme–CNTF Ensembles. The FDH–CNTF ensembles prepared using 3 mg mL^{-1} FDH solution exhibited superior electrocatalytic activity for fructose oxidation in stirred conditions (Figure 4a). The current density of the eCNTF film reached 8 mA cm^{-2} at 0.6 V. In addition, the shrinkage of the area to one-half of the original (see Figure 3c for 3 mg mL^{-1}) boosted the current density by a factor of 2, ca. 16 mA cm^{-2}, indicating that the eCNTF can shrink to the e^2CNTF without significant loss of enzyme activity. Even in quiescent conditions, the current density reached 11 mA cm^{-2} at 0.6 V (Supporting Information, Figure S3). These high current densities of e^2CNTF films indicate an effective interfacing of the enzymes with the large intrasurface of the shrunken CNTF films. In contrast, probably due to the limited loading of enzymes, the conventional random CNT electrode showed a low current density of only ~0.4 mA cm^{-2} (not shown), in agreement with previous reports of conventional CNT aggregate-based enzyme electrodes.[22,23]

The electrode performance depended on the concentration of FDH solution used for preparing e^2CNTFs, as shown in Figure 4b. Among the conditions we studied, the best performance was reproducibly obtained from the e^2CNTF electrode prepared from 3 mg mL^{-1} FDH solution, which contains ca. 1.5 μg FDH (see Figure 3b). This value of FDH content represents one-quarter of the limiting value (6.2 μg) and can be modeled as a linear arrangement of FDH molecules trapped between the CNTs (Figure 2c). At higher contents of FDH, the current values decreased, probably because the overloaded enzymes failed to interface effectively with the CNTs. To investigate enzyme activity within the e^2CNTF films, the apparent Michaelis–Menten constant ($K_{m,app}$) was estimated from the currents at various fructose concentrations using the Lineweaver–Burke equation[24,25] (Figure 5). The derived $K_{m,app}$ was around 10 mM, which is in agreement with the K_m value for the reaction in the bulk solution,[26] indicating that the nanospace formed by CNTF shrinkage could maintain the nature of the FDH enzyme.

Construction of Biofuel Cells. To construct biofuel cells using a FDH-based anode, we prepared a LAC-entrapped CNTF

dx.doi.org/10.1021/ja111517e |J. Am. Chem. Soc. 2011, 133, 5129–5134

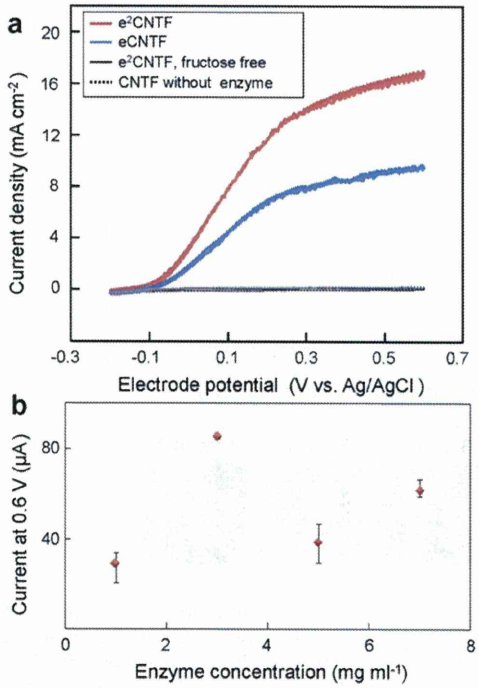

Figure 4. (a) Cyclic voltammograms at 10 mV s^{-1} in the stirred buffer containing 200 mM fructose for the enzyme-adsorbed as-grown CNTF (eCNTF) and the enzyme-entrapped CNTF (e^2CNTF); both were prepared using 12 μm thick CNTF films and 3 mg mL^{-1} FDH solution. The control experiments (enzyme-free or fructose-free) are also shown. The area of one side of the film (1 mm^2 for eCNTF and 0.5 mm^2 for e^2CNTF) was used to the calculation of current density, as validated in the Experimental Section (Electrochemical Measurements) by using Supporting Information, Figure S2. (b) Currents at 0.6 V vs Ag/AgCl of the e^2CNTF films prepared from FDH solutions of different concentrations. The experiments were carried out three times for each condition.

cathode for O_2 reduction. The optimized LAC solution (0.25 mg mL^{-1}) was perfused into a 20 μm thick CNTF film, followed by shrinkage to one-third of the original area (~0.3 mm^2). Cyclic voltammograms of the e^2CNTF showed O_2 reduction at a potential more negative than 0.67 V with a maximum current density of ca. 2 mA cm^{-2} in stirred condition (Figure 6a). From the separate 7 experiments using different LAC-e^2CNTF electrodes, the average of current density was found to be 2.1 ± 0.3 mA cm^{-2}. A further increase in current density to ca. 4 mA cm^{-2} was achieved by overlapping two pieces of e^2CNTF by taking advantage of their free-standing character. By connecting this cathode with the FDH-based anode (Figure 6b), the fuel cell performance was evaluated in an O_2-saturated McIlvaine buffer containing 200 mM fructose. Figure 6c shows the typical power–voltage and current–voltage curves plotted on the basis of the cell voltage upon changing the external resistance (1 kΩ ~ 2 MΩ). The open-circuit voltage of the cell was 0.77 V in agreement with the difference between the potentials at which fructose oxidation and oxygen reduction start to occur on cyclic voltammetries (−0.1 V in Figure 4a and 0.67 V in Figure 6a, respectively). The maximum current density of the cell was ca. 4.8 mA cm^{-2} by reflecting the performance of the present LAC-based cathode. The power density reached 1.8 mW cm^{-2} (at 0.45 V)

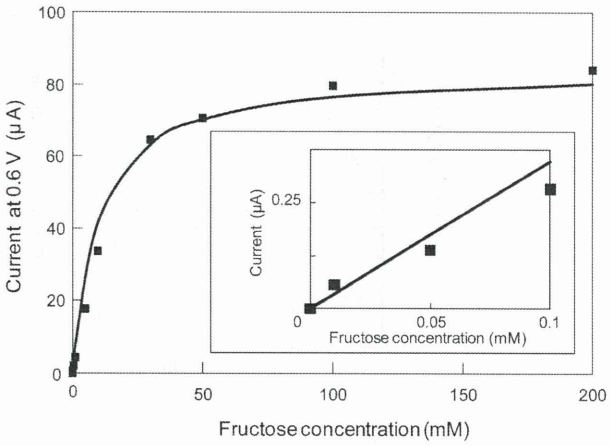

Figure 5. The oxidation currents as a function of the fructose concentration, measured at 0.6 V vs Ag/AgCl in stirred McIlvaine buffer (pH 5.0) for the e^2CNTF electrode prepared using a 12 μm thick CNTF and 3 mg mL^{-1} FDH solution.

in stirred condition, 84% of which could be maintained after continuous operation for 24 h, as shown in Figure 6d.

Application of Enzyme–CNTF Ensemble Films To Power a LED Device. The "free-standing and flexible" character of the present enzyme electrode is its most attractive advantage from a practical viewpoint. The application of such e^2CNTF electrodes for flexible and miniature biodevices is demonstrated in Figure 7. Pieces of e^2CNTF films were patched on an O_2 plasma-treated gold pattern on a polyethylene terephthalate (PET) substrate. After being air dried, the e^2CNTF films remained attached while being bent and immersed in a solution. Similarly, the e^2CNTF films can be wound on the electric leads of a light-emitting diode (LED) device, whose blinking interval is inversely proportional to the power of the biofuel cell. The leads of the LED device were immersed in O_2-saturated stirred McIlvaine buffer (pH 5.0) containing 200 mM fructose. The blinking interval of the LED driven by the e^2CNTF-wound anode and cathode (0.24 s) was similar to that when the e^2CNTF film were merely clamped on the leads without winding (0.20 s), which indicates that the e^2CNTF electrodes maintained their performance in the stressed wound conditions. This unique e^2CNTF-wound needle-type bioelectrode will also be applicable to advanced biosensors and medical devices.[27,28]

■ CONCLUSION

The results presented here show the controlled entrapment of enzymes inside CNTF films through liquid-induced shrinkage. This provides a first example of an enzyme electrode that automatically regulates its intrananospace in response to enzymes to be immobilized. The proposed "in-situ regulation" is a straightforward approach to avoid the longstanding difficulty in the postmodification of enzymes into conventional nanostructured electrodes. In addition, the prepared e^2CNTF film is the first free-standing, flexible enzyme electrode. We demonstrate its use in miniature biofuel cells in patch and wound forms. This free-standing character should also be a significant advantage for other miniature biodevices, such as biosensors. The e^2CNTF film electrodes exhibited reproducible activity in the mA cm^{-2} range. The biofuel cells with e^2CNTF films retained ~80% output at

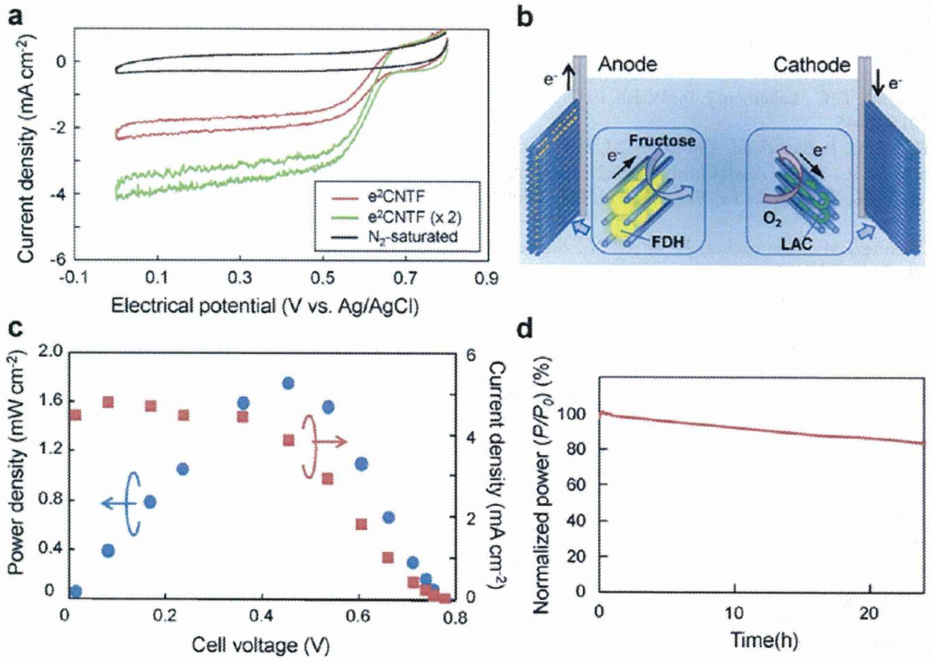

Figure 6. (a) Typical cyclic voltammograms of LAC-entrapped e^2CNTF films (single piece and overlapped double pieces) at 10 mVs^{-1} in O_2-saturated stirred McIlvaine buffer (pH 5.0). The electrode films were prepared using 20 μm thick CNTF film and 0.25 mg mL^{-1} LAC solution. The area of one side of the e^2CNTF film (0.3 mm^2 for both single and overlapped double films) was used for the calculation of current density, as validated in the Experimental Section (Electrochemical Measurements) by using Supporting Information, Figure S2. (b) Schematic of e^2CNTF-based biofuel cell structure. (c) Performance of a biofuel cell composed of a FDH−e^2CNTF anode and the LAC−e^2CNTF cathode in O_2-saturated stirred McIlvaine buffer (pH 5.0) containing 200 mM fructose. The area of one side of the cathode film (0.3 mm^2) was used for the calculation of current and power densities. (d) Dependence of relative stability of power (%) on time with external load of 35.3 kΩ, which is the condition for the maximum power in (c).

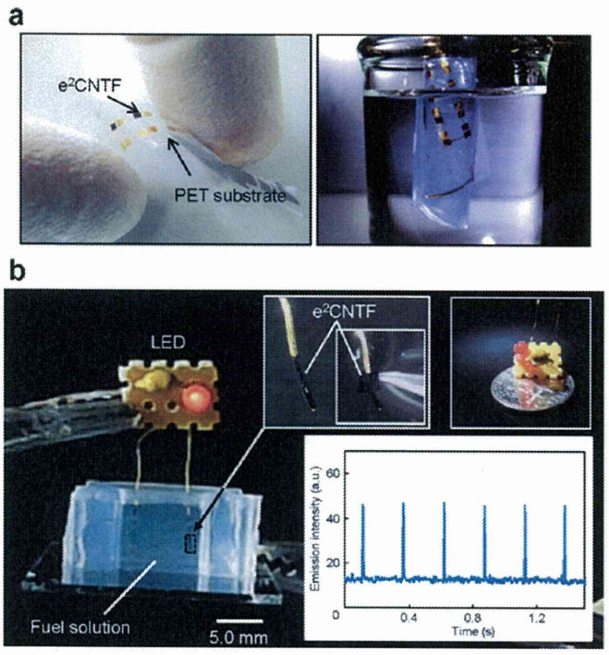

Figure 7. (a) Photographs of e^2CNTF films patched to a flexible PET substrate. The films remained attached while being rolled and immersed in water. (b) Photographs of e^2CNTF films wound on the electric leads of the LED device. The inset shows the time course of the emission intensity of an LED driven by the e^2CNTF-wound anode and cathode.

the mW cm^{-2} level for more than 1 day. To further enhance the cell performance, we intend to create end and sidewall openings in the CNTs by preheating to 600 °C,[17] allowing more efficient flow through the CNTF. The present in situ regulation approach is also applicable for co-entrapment of multiple kinds of enzymes for multifuel or multistep oxidation systems.[29,30]

■ ASSOCIATED CONTENT

Supporting Information. Details of the synthesized CNTF (PDF), a movie of LED emission (MPG), and data of electrochemical measurement (PDF). This material is available free of charge via the Internet at http://pubs.acs.org.

■ AUTHOR INFORMATION

Corresponding Author
nishizawa@biomems.mech.tohoku.ac.jp

■ ACKNOWLEDGMENT

This work was supported by a Core Research for Evolutional Science and Technology grant from the Japan Science and Technology Agency and by a Grant-in-Aid for Creative Scientific Research (Creation of Nano Energetic Systems) from the Ministry of Education, Science and Culture, Japan.

REFERENCES

(1) Mano, N.; Mao, F.; Heller, A. *J. Am. Chem. Soc.* **2003**, *125*, 6588–6594.
(2) Bullen, R. A.; Arnot, T. C.; Lakeman, J. B.; Walsh, F. C. *Biosens. Bioelectr.* **2006**, *21*, 2015–2045.
(3) Kim, J.; Jia, H.; Wang, P. *Biotechnol. Adv.* **2006**, *24*, 296–308.
(4) Wang, J.; Lin, Y. *TrAC, Trends Anal. Chem.* **2008**, *27*, 619–626.
(5) Willner, I.; Yan, Y. M.; Willner, B.; Tel-Vered, R. *Fuel Cells* **2009**, *1*, 7–24.
(6) Gellett, W.; Kesmez, M; Schumacher, J.; Akers, N.; Minteer, S. D. *Electroanalysis* **2010**, *22*, 727–731.
(7) Togo, M.; Takamura, A.; Asai, T.; Kaji, H.; Nishizawa, M. J. *Power Sources* **2008**, *178*, 53–58.
(8) Miyake, T.; Oike, M.; Yoshino, S.; Yatagawa, Y.; Haneda, K.; Nishizawa, M. *Lab Chip* **2010**, *10*, 2574–2578.
(9) Moehlenbrock, M. J.; Minteer, S. D. *Chem. Soc. Rev.* **2008**, *37*, 1188–1196.
(10) Katz, E.; Willner, I. *Chem. Phys. Chem.* **2004**, *5*, 1084–1104.
(11) Gao, F.; Viry, L.; Maugey, M.; Poulin, P.; Mano, N. *Nat. Commun.* **2010**, *1*, 2.
(12) Kamitaka, Y.; Tsujimura, S.; Setoyama, N.; Kajino, T.; Kano, K. *Phys. Chem. Chem. Phys.* **2007**, *9*, 1793–1801.
(13) Sakai, H.; Nakagawa, T.; Tokita, Y.; Hatazawa, T.; Ikeda, T.; Tsujimura, S.; Kano, K. *Energy Environ. Sci.* **2009**, *2*, 133–138.
(14) Tsujimura, S.; Nishina, A.; Hamano, Y.; Kano, K.; Shiraishi, S. *Electrochem. Commun.* **2010**, *12*, 446–449.
(15) Hata, K.; Futaba, D. N.; Mizuno, K.; Namai, T.; Yumura, M.; Iijima, S. *Science* **2004**, *306*, 1362–1364.
(16) Futaba, D. N.; Hata, K.; Yamada, T.; Hiraoka, T.; Hayamizu, Y.; Kakudate, Y.; Tanaike, O.; Hatori, H.; Yumura, M.; Iijima, S. *Nat. Mater.* **2006**, *5*, 987–994.
(17) Hiraoka, T.; Izadi-Najafabadi, A.; Yamada, T.; Futaba, D. N.; Yasuda, S.; Tanaike, O.; Hatori, H.; Yumura, M.; Iijima, S.; Hata, K. *Adv. Funct. Mater.* **2010**, *20*, 422–428.
(18) Fournier, J.; Miousse, D.; Brossard, L.; Menard, H. *Mater. Chem. Phys.* **1995**, *42*, 181–187.
(19) Losic, D.; Shapter, J. G.; Gooding, J. J. *Langmuir* **2002**, *18*, 5422–5428.
(20) Tominaga, M.; Shirakihara, C.; Taniguchi, I. *J. Electroanal. Chem.* **2007**, *610*, 1–8.
(21) Piontek, K.; Antorini, M.; Choinowski, T. *J. Biol. Chem.* **2002**, *277*, 37663–37669.
(22) Wu, X.; Zhao, F.; Varcoe, J. R.; Thumser, A. E.; Avignone-Rossa, C.; Slade, R. C. T. *Biosens. Bioelectr.* **2009**, *25*, 326–331.
(23) Zhao, X.; Jia, H.; Kim, J.; Wang, P. *Biotechnol. Bioeng.* **2009**, *104*, 1068–1074.
(24) Kamin, R. A.; Wilson, G. S. *Anal. Chem.* **1980**, *52*, 1198–1205.
(25) Tominaga, M.; Nomura, S.; Taniguchi, I. *Biosens. Bioelectr.* **2009**, *24*, 1184–1188.
(26) Ameyama, M.; Shinagawa, E.; Matsushita, K.; Adachi, O. *J. Bacteriol.* **1981**, *145*, 814–823.
(27) Heller, A.; Feldman, B. *Chem. Rev.* **2008**, *108*, 2482–2505.
(28) Wei, X.; Liu, J. *Front Energy Power Eng. China* **2008**, *2*, 1–13.
(29) Palmore, G. T. R.; Bertschy, H.; Bergens, S. H.; Whitesides, G. M. *J. Electroanal. Chem.* **1998**, *443*, 155–161.
(30) Arechederra, R. L.; Minteer, S. D. *Fuel Cells* **2009**, *1*, 63–69.

KOKUYO セホ-50B